Mathematical Biosciences and Engineering

http://www.aimspress.com/journal/mbe

MBE, 22(7): 1653–1679.
DOI: 10.3934/mbe.2025061
Received: 26 January 2025
Revised: 22 April 2025
Accepted: 13 May 2025
Published: 21 May 2025

Research article

Optimal therapy schedule of chimeric antigen receptor (CAR) T cell immunotherapy

Ruohan Li[1] **and Jinzhi Lei**[1,2,*]

[1] School of Mathematical Sciences, Tiangong University, Tianjin 300387, China
[2] Center for Applied Mathematics, Tiangong University, Tianjin 300387, China

* **Correspondence:** Email: jzlei@tiangong.edu.cn.

Abstract: Chimeric antigen receptor (CAR) T-cell therapy is a personalized immunotherapy approach in which a patient's T cells are genetically engineered to express synthetic receptors that specifically recognize and target tumor-associated antigens. This approach has demonstrated remarkable success in treating B-cell malignancies by directing CAR-T cells against the CD19 protein. However, treatment efficacy is influenced by the composition and distribution of CAR-T cell subsets administered to the patient. To investigate the impact of different CAR-T cell subtypes and infusion strategies, we developed a mathematical model that captures the dynamic interactions between tumor cells and CAR-T cells within the tumor immune microenvironment. Through computational simulations, we explored how varying the dosage and subtype proportions of infused CAR-T cells affects tumor dynamics and therapeutic outcomes. Our findings highlight the critical role of CAR-T cell subset composition in optimizing treatment efficacy, underscoring the necessity of precise dosing control and tailored infused strategies to maximize therapeutic success.

Keywords: B-ALL; tumor-immune microenvironment; CAR-T therapy; mathematical model; optimal therapy

1. Introduction

Diffuse large B-cell lymphoma (DLBCL) is an aggressive subtype of non-Hodgkin lymphoma originating from B-cells. It primarily affects the lymph nodes, spleen, and liver and represents a significant burden in clinical oncology, with approximately 150,000 new cases diagnosed annually worldwide. The current standard first-line treatment for DLBCL is the R-CHOP regimen, which consists of rituximab, cyclophosphamide, doxorubicin, vincristine, and prednisone. This combination has been the cornerstone of DLBCL therapy, achieving long-term remissions in over 60% of patients with advanced-stage disease [1]. However, approximately 30% of the patients experience disease relapse following

treatment. In recent years, chimeric antigen receptor (CAR) T-cell therapy targeting CD19 has emerged as a promising treatment option for relapsed or refractory DLBCL, demonstrating significant clinical efficacy [2–4].

CAR-T therapy, a form of adoptive cell therapy, was first conceptualized by Gross et al. in 1989 [5] and has since shown remarkable success in treating B-cell lymphomas [6–8]. Over the past decades, rapid advancements in CAR-T technology culminated in the first FDA approval of CAR-T cell therapy in 2017, marking a milestone in cancer immunotherapy [4, 9]. The therapy involves genetically engineering a patient's T cells to express synthetic receptors that specifically recognize and target tumor-associated antigens while preserving their intrinsic immune functionality [4]. This engineering process enhances CAR-T cells' antigen specificity and enables a durable antitumor response [10].

The application of mathematical models in studying CAR-T cell therapy has gained increasing attention in recent years, driven by the growing volume of clinical trial data [11–13]. Sahoo et al. [14] employed a mathematical model based on predator-prey dynamics to investigate the kinetics of CAR-T cell-mediated tumor killing in glioma. The model incorporates key biological processes, including cancer cell proliferation, CAR-T cell expansion, cytotoxic activity, exhaustion, and persistence. Parameter estimation was performed using patient-derived and engineered cancer cell lines analyzed with an *in vitro* real-time cell analyzer. This approach enabled the prediction of therapeutic efficacy as well as the dependence of treatment outcomes on CAR-T cell dosage and target antigen levels.

Kirouac et al. [15] examined the pharmacological properties of engineered T cells from a quantitative pharmacology perspective. By systematically analyzing factors such as drug formulation, pharmacokinetics, and pharmacodynamics, they characterized the impact of varying T cell infusion doses on survival time, expansion dynamics, and tumor cell killing activity. Their findings indicate that insufficient CAR-T cell doses fail to achieve effective tumor control, while excessively high doses can lead to severe adverse effects, including cytokine release syndrome (CRS).

Barros et al. [16] developed a mathematical model that emphasizes the interactions between effector and memory CAR-T cells and tumor cells, highlighting the critical role of memory pool formation in therapeutic response. Building on this framework, Paixão et al. [17] refined the model by categorizing CAR-T cells into three distinct phenotypes: functional, memory, and exhausted CAR-T cells. Their extended model integrates tumor evolution with CAR-T cell differentiation, offering a more comprehensive representation of treatment dynamics. However, the kinetic and metabolic mechanisms governing CAR-T cell therapy remain complex. The therapeutic efficacy of CAR-T cell infusion is also influenced by the functional heterogeneity of T-cell subtypes [18], including the immunosuppressive role of regulatory T cells, the rapid recall response of memory T cells, and the differentiation of effector T cells into memory cells. Furthermore, uncertainties related to T-cell differentiation rates and tumor microenvironment dynamics may impact the predictive accuracy of mathematical models.

CAR-T therapy has demonstrated significant clinical benefit for patients with DLBCL who have not responded to standard therapies [6–8]. Emerging evidence suggests that variations in T-cell subsets, along with patient-specific factors, play a critical role in determining the success of CAR-T therapy [19–21]. However, much of the current research has often overlooked the specific contributions of different CAR-T cell subtypes to therapeutic effectiveness, leading to oversimplified models that fail to accurately capture the complexity of the underlying biological processes [18, 22, 23].

In this study, we developed a mathematical model of CAR-T cell therapy that incorporates the interactions between tumor cells and key CAR-T cell subtypes, including pre-$CD8^+$ CAR-T cells, reg-

ulatory CAR-T cells, and CD4$^+$ CAR-T cells. This model offers a more nuanced simulation of CAR-T cell behavior within the tumor microenvironment. Additionally, our model accounts for changes in the concentration of multiple cytokines and includes differential equations to describe the temporal variations in cytokine levels, capturing their complex roles throughout the treatment process. Using this dynamic model, we quantitatively explored how different initial infusion doses of CAR-T cells influence the dynamics of tumor cell populations. We also identified the optimal dose and ratios of CAR-T cell subtypes required to achieve the best treatment outcomes.

2. Model

2.1. Biological basis

The tumor immune microenvironment comprises various immune cells that either promote or suppress tumor growth, along with cytokines that regulate key signaling pathways. CAR-T therapy involves complex interactions within these microenvironmental components [24].

The infused CAR-T cell population consists of multiple subtypes, including CD4$^+$ CAR-T cells, pre-CD8$^+$ CAR-T cells, effector CAR-T cells, memory CAR-T cells, and regulatory CAR-T cells, each playing a distinct role in the immune response. These CAR-T cells originate from their respective T-cell counterparts extracted from the patient and retain functional similarities to their natural counterparts. CD4$^+$ CAR-T cells, upon stimulation by TGF-β, secrete IL-2, which promotes their own proliferation as well as that of pre-CD8$^+$ CAR-T cells [25]. In response to IL-6 and IFN-γ, released by tumor cells or other immune cells, pre-CD8$^+$ CAR-T cells differentiate into effector CAR-T cells [26, 27]. Effector CAR-T cells mediate tumor cell lysis by releasing granzyme and IFN-γ, while tumor cells counteract this response by inhibiting IFN-γ production through TGF-β secretion [27, 28]. TGF-β also plays a dual role by activating both tumor cells and regulatory CAR-T cells [26]. Regulatory CAR-T cells function as immunosuppressive agents by inhibiting IFN-γ production and restricting pre-CD8$^+$ CAR-T cell proliferation [29]. In the event of a secondary immune challenge, memory CAR-T cells rapidly differentiate into effector CAR-T cells [30, 31], which subsequently eliminate tumor cells [32, 33]. These interactions form the foundation of CAR-T cell immunotherapy, as illustrated in Figure 1. Furthermore, effector CAR-T cells, memory CAR-T cells, and CD4$^+$ CAR-T cells must engage with tumor antigens to form an activation complex, a process governed by the dynamic equilibrium between CAR-T cell binding and dissociation from tumor cell [34, 35].

The therapeutic efficacy of CAR-T therapy depends on the coordinated action of different CAR-T cell subtypes, which must be infused in optimal proportions. Pre-CD8$^+$ CAR-T cells drive the immune response, effector CAR-T cells execute tumor cell killing, while regulatory CAR-T cells modulate the immune response [36]. The balance among these subtypes is critical for achieving optimal treatment outcomes. While a high proportion of effector CAR-T cells may enhance tumor clearance, their persistence over time is limited. Conversely, an excessive number of regulatory CAR-T cells can lead to heightened immunosuppression, thereby diminishing the therapeutic effect. Therefore, precisely calibrating the infusion ratios of CAR-T cell subtypes is essential for maximizing treatment efficacy [18, 37].

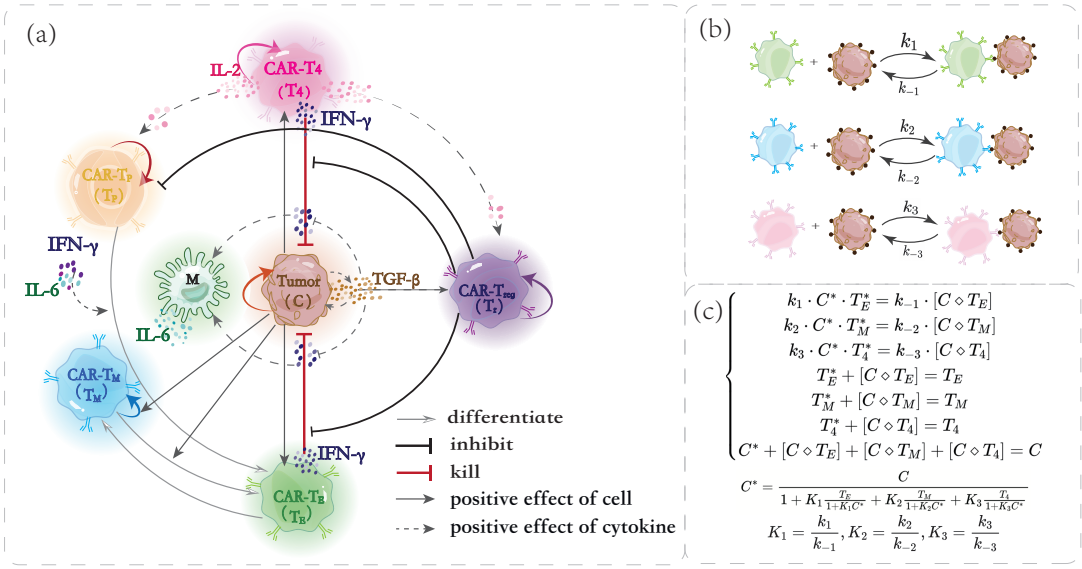

Figure 1. Diagram of CAR-T cell interactions. (a) CD4$^+$ CAR-T cells proliferate in response to IL-2 stimulation. IL-2 also promotes the proliferation of pre-CD8$^+$ CAR-T cells and regulatory CAR-T (CAR-T$_{\text{reg}}$) cells. Pre-CD8$^+$ CAR-T cells differentiate into effector CAR-T cells under the influence of IL-6 and IFN-γ. Effector CAR-T cells and CD4$^+$ CAR-T cells, upon stimulation by tumor cells, secrete IFN-γ, which contributes to tumor killing. Macrophages are responsible for IL-6 production. CAR-T$_{\text{reg}}$ cells suppress the proliferation of pre-CD8$^+$ CAR-T cells and inhibit the tumor-killing activity of effector and CD4$^+$ CAR-T cells. Additionally, tumor cells release TGF-β to counteract their own destruction by effector and CD4$^+$ CAR-T cells. (b) Schematic representation of the dynamic binding and dissociation of effector CAR-T cells, memory CAR-T cells, and CD4$^+$ CAR-T cells with tumor cells. (c) Dependence of free tumor cell population on CAR-T cell numbers. Here, C^*, T_E^*, T_M^*, and T_4^* represent free tumor cells, free effector CAR-T cells, free memory CAR-T cells, and free CD4$^+$ CAR-T cells, respectively. The parameters k_i and k_{-i} denote the binding and dissociation rates between CAR-T cells and tumor cells. The notations $[C \diamond T_E]$, $[C \diamond T_M]$, and $[C \diamond T_4]$ represent the complexes formed between tumor cells and effector CAR-T cells, memory CAR-T cells, and CD4$^+$ CAR-T cells, respectively.

2.2. *Mathematical formulation*

2.2.1. Equation for CD4$^+$ CAR-T cells

CD4$^+$ CAR-T cells, denoted as T_4, originate from CD4$^+$ T cells and play a critical role in recognizing and eliminating tumor cells. Additionally, they secrete interleukin-2 (IL-2, denoted as I_2), which enhances their proliferation. The population dynamics of CD4$^+$ CAR-T cells are governed by the following equation:

$$\frac{\mathrm{d}T_4}{\mathrm{d}t} = \underbrace{\lambda_{T_4 I_2} \frac{I_2}{K_{I_2} + I_2} T_4}_{\text{proliferation by IL-2}} - \underbrace{d_{T_4} T_4}_{\text{death}}. \tag{2.1}$$

Here, $\lambda_{T_4 I_2}$ is the maximum proliferation rate of CD4$^+$ CAR-T cells in response to IL-2, K_{I_2} is the half-saturation constant for IL-2, and d_{T_4} represents the apoptosis rate of CD4$^+$ CAR-T cells.

2.2.2. Equation for pre-CD8$^+$ CAR-T cells

Pre-CD8$^+$ CAR-T cells (CAR-T$_{\mathrm{P}}$, denoted as T_P), derived from naïve T cells, proliferate in response to IL-2 stimulation. However, their proliferation is suppressed by regulatory CAR-T cells (CAR-T$_{\mathrm{reg}}$, denoted as T_r). In the presence of interleukin-6 (IL-6, I_6) and interferon-gamma (IFN-γ, I_γ), pre-CD8$^+$ CAR-T cells differentiate into effector CAR-T cells. The following equation describes the dynamics for pre-CD8$^+$ CAR-T cells:

$$\begin{aligned}\frac{\mathrm{d}T_P}{\mathrm{d}t} = & \underbrace{\lambda_{T_P I_2}\frac{I_2}{K_{I_2}+I_2}}_{\text{proliferation by IL-2}} \times \underbrace{\frac{1}{1+T_r/K_{T_r}}}_{\text{inhibition by CAR-T}_{\mathrm{reg}}} \times T_P \\ & - \underbrace{\lambda\left(\frac{I_6}{K_{I_6}+I_6}+\frac{I_\gamma}{K_{I_\gamma}+I_\gamma}\right)T_P}_{\text{CAR-T}_{\mathrm{P}}\rightarrow\text{CAR-T}_{\mathrm{E}}\text{ under IL-6 and IFN-}\gamma} - \underbrace{d_{T_P}T_P}_{\text{death}}.\end{aligned} \tag{2.2}$$

Here, $\lambda_{T_P I_2}$ represents the maximum proliferation rate of pre-CD8$^+$ CAR-T cells in response to IL-2 simulation, K_{I_2} is the half-saturation constant of IL-2, K_{T_r} is the half-saturation constant for regulatory CAR-T cells, λ denotes the conversion rate of pre-CD8$^+$ CAR-T cells into effector CAR-T cells in response to IL-6 and IFN-γ, and d_{T_P} is the apoptosis rate of pre-CD8$^+$ CAR-T cells.

2.2.3. Equation for effector CAR-T cells

Effector CAR-T cells (CAR-T$_{\mathrm{E}}$, denoted as T_E) are derived from pre-CD8$^+$ CAR-T cells under the stimulation of IL-6 and IFN-γ. These cells play a critical role in eliminating tumor cells. As immunotherapy progresses and the tumor burden decreases, some effector CAR-T cells transition into memory CAR-T cells (CAR-T$_{\mathrm{M}}$, denoted as T_M), which persist in the body and can be rapidly reactivated upon tumor recurrence. Memory CAR-T cells, when exposed to tumor antigens, differentiate back into effector CAR-T cells to mount an immune response. This dynamic process is described by the following equation:

$$\begin{aligned}\frac{\mathrm{d}T_E}{\mathrm{d}t} = & \underbrace{\lambda\left(\frac{I_6}{K_{I_6}+I_6}+\frac{I_\gamma}{K_{I_\gamma}+I_\gamma}\right)T_P}_{\text{CAR-T}_{\mathrm{P}}\rightarrow\text{CAR-T}_{\mathrm{E}}\text{ under IL-6 and IFN-}\gamma} + \underbrace{\lambda_{T_{M\rightarrow E}}\frac{K_2 C^*}{1+K_2 C^*}T_M}_{\text{CAR-T}_{\mathrm{M}}\rightarrow\text{CAR-T}_{\mathrm{E}}\text{ under tumor stimuli}} \\ & - \underbrace{\lambda_{T_{E\rightarrow M}}T_E}_{\text{CAR-T}_{\mathrm{E}}\rightarrow\text{CAR-T}_{\mathrm{M}}} - \underbrace{d_{T_E}T_E}_{\text{death}}.\end{aligned} \tag{2.3}$$

Here, λ represents the conversion rate of pre-CD8$^+$ CAR-T cells to effector CAR-T cells under IL-6 and IFN-γ, $\lambda_{T_M\rightarrow E}$ denotes the reactivation rate of memory CAR-T cells in response to tumor presence, $\lambda_{T_E\rightarrow M}$ is the transition rate of effector CAR-T cells back into memory CAR-T cells, d_{T_E} is the apoptosis rate of effector CAR-T cells, and C^* represents the number of free tumor cells that are not bound to CAR-T cells, determined by the equilibrium equation (refer to Figure 1(c)):

$$C^* = \frac{C}{1+K_1\frac{T_E}{1+K_1C^*}+K_2\frac{T_M}{1+K_2C^*}+K_3\frac{T_4}{1+K_3C^*}}. \tag{2.4}$$

Tumor cells can bind to different types of CAR-T cells (effector, memory, or $CD4^+$ CAR-T cells), leading to competition for binding sites on the tumor surface. The availability of free tumor cells (C^*) influences the transition of memory CAR-T cells back into effector CAR-T cells. This binding and dissociation process is illustrated in Figure 1(c), which provides a mathematical formulation for the number of unbound tumor cells.

2.2.4. Equation for memory CAR-T cells

Memory CAR-T cells (CAR-T_M, denoted as T_M) are long-lived immune cells that serve as a reservoir for rapid immune response upon tumor recurrence. Under normal conditions, their population remains low. However, upon antigen stimulation by tumor cells, memory CAR-T cells proliferate and differentiate into effector CAR-T cells. When the tumor burden decreases, some effector CAR-T cells revert to memory CAR-T cells, ensuring long-term immunological surveillance. The dynamics of memory CAR-T cells are governed by the following equation:

$$\begin{aligned}\frac{\mathrm{d}T_M}{\mathrm{d}t} = & \underbrace{\lambda_{T_M}\frac{K_{T_M}}{K_{T_M}+T_M}T_M}_{\text{proliferation}} + \underbrace{\lambda_{T_{E\to M}}T_E}_{\text{CAR-T}_\text{E}\to\text{CAR-T}_\text{M}} - \underbrace{\lambda_{T_{M\to E}}\frac{K_2C^*}{1+K_2C^*}T_M}_{\text{CAR-T}_\text{M}\to\text{CAR-T}_\text{E}} \\ & - \underbrace{d_{T_M}T_M}_{\text{death}}.\end{aligned} \tag{2.5}$$

Here, λ_{T_M} represents the proliferation rate of memory CAR-T cells, $\lambda_{T_E\to M}$ is the conversion rate of effector CAR-T cells into memory CAR-T cells, $\lambda_{T_M\to E}$ is the rate at which memory CAR-T cells differentiate into effector CAR-T cells upon tumor antigen stimulation, K_2 is the equilibrium binding constant for interactions between memory CAR-T cells and tumor cells, d_{T_M} is the apoptosis rate of memory CAR-T cells, and K_{T_M} is the half-saturation constant for memory CAR-T cell proliferation, dependent on the number of free tumor cells:

$$K_{T_M} = K_{T_{M_0}} + K_{T_{M_1}}\frac{K_2C^*}{1+K_2C^*}, \tag{2.6}$$

where $K_{T_{M_0}}$ represents the baseline half-saturation constant in the absence of tumor cells, $K_{T_{M_1}}$ represents the half-saturation constant in the presence of tumor cells, and C^* denotes the concentration of free tumor cells. Equation (2.6) captures the dynamic balance between memory and effector CAR-T cells, regulated by tumor burden and antigen stimulation.

2.2.5. Equation for regulatory CAR-T cells

Regulatory CAR-T cells (CAR-T_{reg}, denoted as T_r) are derived from regulatory T cells, a class of immunosuppressive cells that modulate the immune response. These cells proliferate in response to IL-2 and exert immunosuppressive effects, thereby influencing the immune microenvironment. The dynamics of regulatory CAR-T cells are governed by the following equation:

$$\frac{\mathrm{d}T_r}{\mathrm{d}t} = \underbrace{\lambda_{T_rI_2}\frac{I_2}{I_2+K_{I_2}}T_r}_{\text{proliferation by IL-2}} - \underbrace{d_{T_r}T_r}_{\text{death}}. \tag{2.7}$$

Here, $\lambda_{T_rI_2}$ represents the proliferation rate of regulatory CAR-T cells in response to IL-2, K_{I_2} is the half-saturation constant for IL-2, and d_{T_r} denotes the apoptosis rate of regulatory CAR-T cells.

2.2.6. Equation for tumor cells

This study focuses on diffuse large B-cell lymphoma (DLBL), a type of B-cell lymphoma characterized by rapid proliferation. Tumor cells, denoted by C, are targeted by effector CAR-T cells and CD4$^+$ CAR-T cells, though their elimination is inhibited by immunosuppressive regulatory CAR-T cells. The following equation governs the tumor cell population:

$$\begin{aligned}\frac{\mathrm{d}C}{\mathrm{d}t} = & \underbrace{\lambda_C \frac{K_C}{K_C + C} C}_{\text{proliferation}} - \underbrace{d_C C}_{\text{death}} \\ & - \underbrace{k_{T_E} \frac{K_1 T_E}{1 + K_1 T_E^* + K_2 T_M^* + K_3 T_4^* + K_1 C}}_{\text{killing by CAR-T}_\text{E}} \times \underbrace{\frac{1}{1 + T_r / K_{T_r}}}_{\text{inhibition by CAR-T}_\text{reg}} \times C \\ & - \underbrace{k_{T_4} \frac{K_3 T_4}{1 + K_1 T_E^* + K_2 T_M^* + K_3 T_4^* + K_1 C}}_{\text{killing by CAR-T}_4} \times \underbrace{\frac{1}{1 + T_r / K_{T_r}}}_{\text{inhibition by CAR-T}_\text{reg}} \times C,\end{aligned} \tag{2.8}$$

where

$$T_E^* = \frac{T_E}{1 + K_1 C^*}, \quad T_M^* = \frac{T_M}{1 + K_2 C^*}, \quad T_4^* = \frac{T_4}{1 + K_3 C^*}.$$

In this equation, λ_C represents the tumor cell proliferation rate, and d_C denotes the natural apoptosis rate of tumor cells. The parameters k_{T_E} and k_{T_4} quantify the killing efficiency of effector CAR-T cells and CD4$^+$ CAR-T cells, respectively. The constants K_1, K_2, and K_3 describe the equilibrium binding and dissociation rates of effector CAR-T cells, memory CAR-T cells, and CD4$^+$ CAR-T cells with tumor cells. Additionally, T_E^*, T_M^*, and T_4^* denote the fractions of free effector CAR-T cells, free memory CAR-T cells, and free CD4$^+$ CAR-T cells, respectively (Figure 1(c)). The term K_{T_r} represents the half-saturation constant of regulatory CAR-T cells, which mediate the immune suppression. The inhibition terms account for the suppressive effect of regulatory CAR-T cells on tumor elimination by CAR-T therapy.

In Eq (2.8), a Hill function with a saturation K_C is used to model the proliferation of tumor cells. The Hill-type growth rate arises from the regulation of cell proliferation through cytokine-mediated signaling pathways. Biologically, these cytokines may be secreted by the cells themselves and inhibit proliferation or be released from the surrounding niche to promote it. In either case, the proliferation rates can be described by a Hill-type function of the cell number. For a mathematical derivation of the Hill-type growth rate, refer to Lei [38] or Bernard et al. [39].

2.2.7. Equation for macrophages

Macrophages, denoted as M, arise from monocytes in response to IFN-γ, playing a key role in tumor immune response through IL-6. The equation governing macrophage dynamics is given by:

$$\frac{\mathrm{d}M}{\mathrm{d}t} = \underbrace{\lambda_{MI_\gamma} \frac{I_\gamma}{I_\gamma + K_{I_\gamma}} M_0}_{\text{differentiation under IFN-}\gamma} - \underbrace{d_M M}_{\text{death}}, \tag{2.9}$$

where M_0 denotes precursor monocytes, which differentiate into macrophages under IFN-γ stimulation. The parameter λ_{MI_γ} represents the differentiation rate of monocytes into macrophages, while K_{I_γ} is the half-saturation constant of IFN-γ. The term d_M describes the apoptosis rate of macrophages.

2.2.8. Equations for cytokines

Cytokines are small, biologically active proteins secreted by immune and non-immune cells in response to various stimuli. They mediate cell-cell communication and play essential roles in regulating cell growth, differentiation, and immune responses.

IL-2 dynamics

IL-2 is an interleukin that plays a critical role in immune system regulation. It is secreted by $CD4^+$ CAR-T cells and facilitates the proliferation of both pre-$CD8^+$ CAR-T cells and self-renewing $CD4^+$ CAR-T cells. The dynamics of IL-2 are governed by the following equation:

$$\frac{\mathrm{d}I_2}{\mathrm{d}t} = \underbrace{\lambda_{I_2T_4}T_4}_{\text{production by CAR-T}_4} - \underbrace{d_{I_2}I_2}_{\text{degradation}}, \tag{2.10}$$

where $\lambda_{I_2T_4}$ is the production rate of IL-2 by $CD4^+$ CAR-T cells, and d_{I_2} represents its degradation rate.

IFN-γ dynamics

IFN-γ is a key cytokine with antiviral and immunomodulatory properties. It is primarily produced by effector CAR-T cells and $CD4^+$ CAR-T cells, playing a significant role in tumor suppression. However, its secretion is inhibited by regulatory CAR-T cells and transforming growth factor beta (TGF-β). The equation governing IFN-γ dynamics is given by:

$$\begin{aligned}\frac{\mathrm{d}I_\gamma}{\mathrm{d}t} = &\underbrace{(\lambda_{I_\gamma T_E}T_E}_{\text{production by CAR-T}_E} + \underbrace{\lambda_{I_\gamma T_4}T_4)}_{\text{production by CAR-T}_4} \underbrace{(\frac{1}{1+T_r/K_{T_r}} + \frac{1}{1+T_\beta/K_{T_\beta}})}_{\text{inhibition by CAR-T}_{\text{reg}} \text{ and TGF-}\beta} \\ &- \underbrace{d_{I_\gamma}I_\gamma}_{\text{degradation}},\end{aligned} \tag{2.11}$$

where $\lambda_{I_\gamma T_8}$ and $\lambda_{I_\gamma T_4}$ are the production rates of IFN-γ by effector CAR-T cells and $CD4^+$ CAR-T cells, respectively. The parameters K_{T_r} and K_{T_β} denote the half-saturation constants for regulatory CAR-T cells and TGF-β, respectively, while d_{I_γ} represents the degradation rate of IFN-γ.

TGF-β dynamics

TGF-β is a tumor-derived cytokine that promotes tumor progression, activates regulatory CAR-T cells, and suppresses the cytotoxic effects of immune cells. The equation governing its dynamics is:

$$\frac{\mathrm{d}T_\beta}{\mathrm{d}t} = \underbrace{\lambda_{T_\beta C}C}_{\text{production by tumor cells}} - \underbrace{d_{T_\beta}T_\beta}_{\text{degradation}}, \tag{2.12}$$

where $\lambda_{T_\beta C}$ is the production rate of TGF-β by tumor cells, and d_{T_β} represents its degradation rate.

IL-6 dynamics

IL-6 is predominantly secreted by macrophages and plays a crucial role in immune regulation by promoting the differentiation of pre-CD8$^+$ CAR-T cells into effector CAR-T cells. The equation for IL-6 dynamics is given by:

$$\frac{\mathrm{d}I_6}{\mathrm{d}t} = \underbrace{\lambda_{I_6M}M}_{\text{production by macrophages}} - \underbrace{d_{I_6}I_6}_{\text{degradation}}, \tag{2.13}$$

where λ_{I_6M} is the production rate of IL-6 by macrophages, and d_{I_6} is its degradation rate.

2.3. Parameter estimation

Table 1. Default parameter values.

Notation	Description	Value	Range	Reference
$\lambda_{T_4I_2}$	Activation rate of CD4$^+$ CAR-T cells under IL-2	0.25 day^{-1}		
$\lambda_{T_PI_2}$	Activation rate of pre-CD8$^+$ CAR-T cells under IL-2	1.5 day^{-1}	10^{-2}–10^{1}	[40,41]
$\lambda_{T_rI_2}$	Activation rate of regulatory CAR-T cells under IL-2	0.038 day^{-1}		
λ_{MI_γ}	Activation rate of macrophage under IFN-γ	0.25 day^{-1}		
$\lambda_{I_2T_4}$	Production rate of IL-2	0.46×10^{-4} ng ml^{-1} day^{-1}cell^{-1}		
$\lambda_{I_\gamma T_E}$	Production rate of IFN-γ from effector CAR-T cells	0.74×10^{-9} ng ml^{-1} day^{-1} cell^{-1}		
$\lambda_{I_\gamma T_4}$	Production rate of IFN-γ from helper CAR-T cells	0.58×10^{-9} ng ml^{-1} day^{-1} cell^{-1}	10^{-7}–10^{-3}	[42]
$\lambda_{T_\beta C}$	Production rate of TGF-β from tumor	0.11×10^{-4} ng ml^{-1} day^{-1} cell^{-1}		
λ_{I_6M}	Production rate of IL-6 from macrophages	0.52×10^{-5} ng ml^{-1} day^{-1} cell^{-1}		
K_{T_P}	Half-saturation of pre-CD8$^+$CAR-T cell	5.0×10^{7} cells		
K_{T_4}	Half-saturation of regulatory CAR-T cell	1×10^{4} cells	10^{4}–10^{9}	
K_{T_r}	Half-saturation of regulatory CAR-T cell	1×10^{4} cells		[41,43]
K_C	Half-saturation of tumor cells	5×10^{7} cells		
K_{I_2}	Half-saturation of IL-2	1×10^{-1} ng ml^{-1}		
K_{I_6}	Half-saturation of IL-6	2.5×10^{-3} ng ml^{-1}	10^{-5}–10^{-3}	[41]
K_{I_γ}	Half-saturation of IFN-γ	1×10^{-2} ng ml^{-1}		
K_{T_β}	Half-saturation of TGF-β	1×10^{-3} ng ml^{-1}		
λ_C	Proliferation rate of tumor cells	3.3 day^{-1}		[11]
k_{T_E}	Killing rate of tumor cells by effector CAR-T cells	3.57 cells day^{-1}		[11]
λ_{T_M}	Proliferation rate of memory CAR-T cells	0.02 day^{-1}		[16]
$\lambda_{T_{E\to M}}$	Differentiation rate from effector CAR-T cells to memory CAR-T cells	0.26×10^{-4} day^{-1}		[16]
$\lambda_{T_{M\to E}}$	Differentiation rate from memory CAR-T cells to effector CAR-T cells	0.1×10^{-5} day^{-1}		[16]
k_{T_4}	Killing rate of tumor cells by CD4$^+$ CAR-T cells	0.08 cells day^{-1}		[41]

The mathematical model incorporates six classes of tumor-immune-related parameters: naïve immune cell count, cytokine activation rate, cytokine production rate, cytokine degradation rate, apoptosis rate of immune cells, and the half-saturation constants. We estimated these parameters based on values reported in the literature.

For the magnitude of naïve immune cells in the tumor microenvironment, we referred to Zhang [11] and Lai [41], which suggest a range of approximately 10^6–10^8 cells. The cytokine activation rate was estimated based on values reported by Li [46] and Lai [41], which range from 10^{-2} to 10^{1} day^{-1}. For the cytokine production rate, we referred to Robertson-Tessi et al. [42], which reported values between 10^{-7} and 10^{-3} ng ml^{-1} cell^{-1}.

The apoptosis rates of immune cells and the half-saturation constant of immune cells were obtained from multiple studies, which place the apoptosis rate in the range of 10^{-3}–10^{-1} day^{-1} and the half-

saturation constant on the order of 10^4–10^9 cells [40, 43–45]. The apoptosis rate of cytokines, denoted as d, was calculated using the relation $d = \frac{\ln 2}{t_{1/2}}$, where $t_{1/2}$ represents the half-life of the cytokine [46]. The estimated orders of magnitude for these parameters are summarized in Tables 1 and 2.

To refine the parameter estimates, we explore the parameter space and adjust parameter values to achieve tumor evolution dynamics that are comparable to experimental observations.

Table 2. Default parameter values (continued).

Notation	Description	Value	Magnitude	Reference
$K_{T_{M0}}$	Half-saturation of memory CAR-T cell without tumor cells	0.2 cells		
$K_{T_{M1}}$	Half-saturation of memory CAR-T cell under tumor cells	20 cells		
K_1	Dynamic equilibrium constant for the binding and dissociation between effector CAR-T cells and tumor cells	0.05	0–10^1	estimation
K_2	Dynamic equilibrium constant for the binding and dissociation between memory CAR-T cells and tumor cells	0.04		
K_3	Dynamic equilibrium constant for the binding and dissociation between $CD4^+$ CAR-T cells and tumor cells	0.001		
λ	Differentiation rate from pre-$CD8^+$ CAR-T cells to effector CAR-T cells under IL-6 and IFN-γ	0.2 day^{-1}		
d_{T_4}	Death rate of $CD4^+$ CAR-T cells	0.20 day^{-1}		
d_{T_P}	Death rate of pre-$CD8^+$CAR-T cells	0.07 day^{-1}		
d_{T_E}	Death rate of effector CAR-T cells	0.18 day^{-1}		
d_{T_M}	Death rate of memory CAR-T cells	0.0065×10^{-2} day^{-1}	10^{-3}–10^{-1}	[40]
d_{Tr}	Death rate of regulatory CAR-T cells	0.06 day^{-1}		
d_C	Death rate of tumor cells	0.075 day^{-1}		
d_M	Death rate of macrophage	0.03 day^{-1}		
d_{I_2}	Degradation rate of IL-2	7.7 day^{-1}		
d_{T_β}	Degradation rate of TGF-β	5.0 day^{-1}	10^0–10^2	[43–45]
d_{I_γ}	Degradation rate of IFN-γ	4.16 day^{-1}		
d_{I_6}	Degradation rate of IL-6	4.0 day^{-1}		
M_0	The precursor cells of macrophages	1×10^3cells		estimation

3. Results

3.1. Sensitivity analysis

To investigate how tumor progression responds to changes in the model parameters, we performed a global sensitivity analysis, using progression-free survival (PFS) as the primary index. PFS, commonly used in clinical trials and oncology, refers to the length of time a patient with cancer lives without the disease worsening or progressing during and after treatment. In our model, PFS represents the period during which the tumor cell count remains unchanged or does not exceed its initial value, i.e.,

$$\text{PFS} = \sup_{t>0}\{t \mid C(t) \le C(0)\},$$

where $C(t)$ is the tumor cell count at time t, and $C(0)$ is the initial tumor cell count.

For the global sensitivity analysis, we varied all model parameters by ±10% from their default values, generating 1000 sets of parameters. For each parameter set, we fixed the initial condition and solved the model equations. From the resulting solutions, we calculated the corresponding PFS by tracking the evolution of tumor cell counts. The Pearson correlation coefficients between PFS and the model parameters were then computed (Figure 2(a)). The results show that PFS is insensitive to most

parameters, with correlation coefficients ranging between −0.2 and 0.2. However, parameters related to tumor growth (λ_C) and tumor-killing of effector CAR-T cells (k_{TE}) exhibit significant correlations with the PFS. Specifically, λ_C shows a negative correlation, while k_{TE} is positively correlated with PFS. The dependences of PFS on the four key parameters—λ_C, d_C, k_{TE}, and d_{TE}—are illustrated in Figure 2(b).

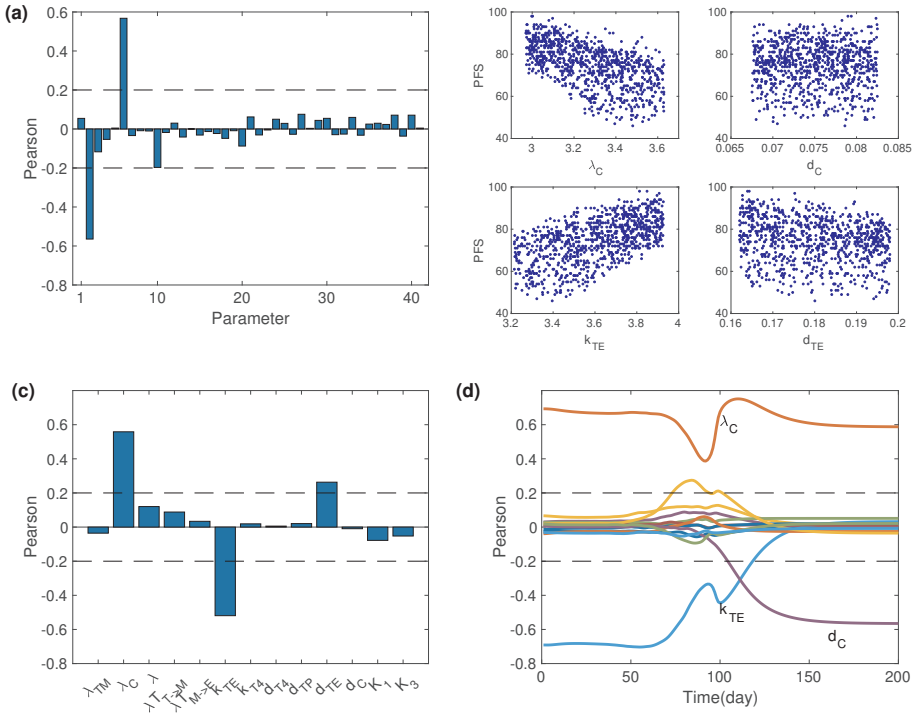

Figure 2. Parametric sensitivity analysis. (a) Pearson correlation coefficient of all parameters concerning PFS after CAR-T treatment. The parameters are listed in Table 3. (b) PFS versus parameters λ_C, d_C, k_{TE}, and d_{TE}. (c) Pearson correlation between tumor cell counts at day 80 for important parameters. (d) Evolution of Pearson correlation between key parameters and tumor cell count over 200 days following CAR-T cell infusion.

To further investigate how the number of tumor cells is affected by changes in specific parameters, we focused on tumor cell number for the sensitivity analysis. The selected parameters were those that could potentially influence tumor progression significantly. These included λ_{T_M} (the proliferation rate of memory CAR-T cells), λ_C (the proliferation rate of tumor cells), λ (the differentiation rate of pre-CD8$^+$CAR-T cells into effector CAR-T cells), $\lambda_{T_{E\to M}}$ (the differentiation rate of effector CAR-T cells into memory CAR-T cells), $\lambda_{T_{M\to E}}$ (the differentiation rate of memory CAR-T cells into effector CAR-T cells), k_{T_E} (the tumor cells killing rate by effector CAR-T cells), k_{T_4} (the tumor cells killing rate by CD4$^+$ CAR-T cells), d_{T_4} (the death rate of CD4$^+$ CAR-T cells), d_{T_P} (the death rate of pre-CD8$^+$CAR-T cells), d_{T_E} (the death rate of effector CAR-T cells), d_C (the death rate of tumor cells), K_1 (the equilibrium rate constants for binding and dissociation of effector CAR-T cells and tumor cells), and K_3 (the equilibrium rate constants for binding and dissociation of CD4$^+$ CAR-T cells and tumor cells).

The Pearson correlations between the parameters and the tumor cell count at 80 days after treatment are shown in Figure 2(c). The results indicate that λ_C is positively correlated with tumor growth, while

k_{T_E} is negatively correlated. To extend the analysis, we considered a longer time frame of 200 days (Figure 2(d)). Over this extended period, λ_C maintains a positive correlation with tumor growth, while k_{T_E} exhibits a moderate negative effect, with a Pearson correlation of −0.05 at day 200. Additionally, the Pearson correlation for the tumor cell death rate d_C shows a moderate negative effect at day 80 but becomes strongly negative at day 200. These findings suggest that the tumor cell killing rate by effector CAR-T cells (k_{T_E}) is crucial for early tumor response, while the tumor cell death rate (d_C) plays a significant role in the final count following tumor relapse.

Table 3. Parameters in Figure 2(a).

Serial No.	1	2	3	4	5	6	7	8	9	10	11
Parameter	λ_{T_M}	λ_C	λ	$\lambda_{T_{E\to M}}$	$\lambda_{T_{M\to E}}$	k_{T_E}	k_{T_4}	d_{T_4}	d_{T_P}	d_{T_E}	dC
Serial No.	12	13	14	15	16	17	18	19	20	21	22
Parameter	K_1	K_2	K_3	$\lambda_{T_4 I_2}$	$\lambda_{T_P I_2}$	$\lambda_{T_r I_2}$	$\lambda_{M I_\gamma}$	$\lambda_{I_2 T_4}$	$\lambda_{I_\gamma T_E}$	$\lambda_{I_\gamma T_4}$	$\lambda_{T_\beta C}$
Serial No.	23	24	25	26	27	28	29	30	31	32	33
Parameter	$\lambda_{I_6 M}$	K_{T_P}	K_{T_4}	K_{T_r}	K_{T_M}	K_{T_2}	K_{T_6}	K_{I_γ}	K_{T_β}	$K_{T_{M_0}}$	$K_{T_{M_1}}$
Serial No.	34	35	36	37	38	39	40	41	42		
Parameter	K_C	M_0	d_M	d_{T_r}	d_{T_M}	d_{I_2}	d_{T_β}	d_{I_γ}	d_{I_6}		

3.2. Threshold effect on the number of effector CAR-T cells

Effector CAR-T cells are crucial for tumor cell elimination, while memory CAR-T cells are vital for sustaining long-term tumor suppression. To explore how tumor progression depends on the number of CAR-T cells infused into the body, we developed a coarse-grained model that describes the interaction among tumor cells, effector CAR-T cells, and memory CAR-T cells. Coarse-grained models provide quick preliminary results, enable more focused and accurate large-scale models, and help to understand the system's underlying behavior. This model captures the key regulatory mechanisms within the tumor microenvironment, as illustrated in Figure 3.

Based on the coarse-grained model shown in Figure 3 and Eqs (2.3), (2.5), and (2.8), the system dynamics are described by the following equations:

$$\frac{\mathrm{d}T_E}{\mathrm{d}t} = \underbrace{\lambda_{T_{M\to E}}\frac{K_2 C^*}{1+K_2 C^*}T_M}_{\text{CAR-T}_\text{M}\to\text{CAR-T}_\text{E}\text{ under tumor cells}} - \underbrace{\lambda_{T_{E\to M}}T_E}_{\text{CAR-T}_\text{E}\to\text{CAR-T}_\text{M}} - \underbrace{d_{T_E}T_E}_{\text{death}}, \tag{3.1}$$

$$\frac{\mathrm{d}T_M}{\mathrm{d}t} = \underbrace{\lambda_{T_M}\frac{K_{T_M}}{K_{T_M}+T_M}T_M}_{\text{proliferation}} + \underbrace{\lambda_{T_{E\to M}}T_E}_{T_E\to T_M} - \underbrace{\lambda_{T_{M\to E}}\frac{K_2 C^*}{1+K_2 C^*}T_M}_{T_M\to T_E} - \underbrace{d_{T_M}T_M}_{\text{death}}, \tag{3.2}$$

$$\frac{\mathrm{d}C}{\mathrm{d}t} = \underbrace{\lambda_C\frac{K_C}{K_C+C}C}_{\text{proliferation}} - \underbrace{k_{T_E}\frac{K_1 T_E^*}{1+K_1 T_E^*+K_2 T_M^*+K_1 C}C}_{\text{killing by T}_\text{E}} - \underbrace{d_C C}_{\text{death}}, \tag{3.3}$$

where

$$C^* = \frac{C}{1 + K_1 \frac{T_E}{1+K_1 C^*} + K_2 \frac{T_M}{1+K_2 C^*}},$$

$$K_{T_M} = K_{T_{M_0}} + K_{T_{M_1}} \frac{K_2 C^*}{1 + K_2 C^*},$$

$$T_E^* = \frac{T_E}{1 + K_1 C^*}, \quad T_M^* = \frac{T_M}{1 + K_2 C^*}.$$

To assess the impact of CAR-T cell infusion on tumor progression, we varied the initial numbers of effector and memory CAR-T cells and solved the equations to evaluate the dynamics of tumor cell growth.

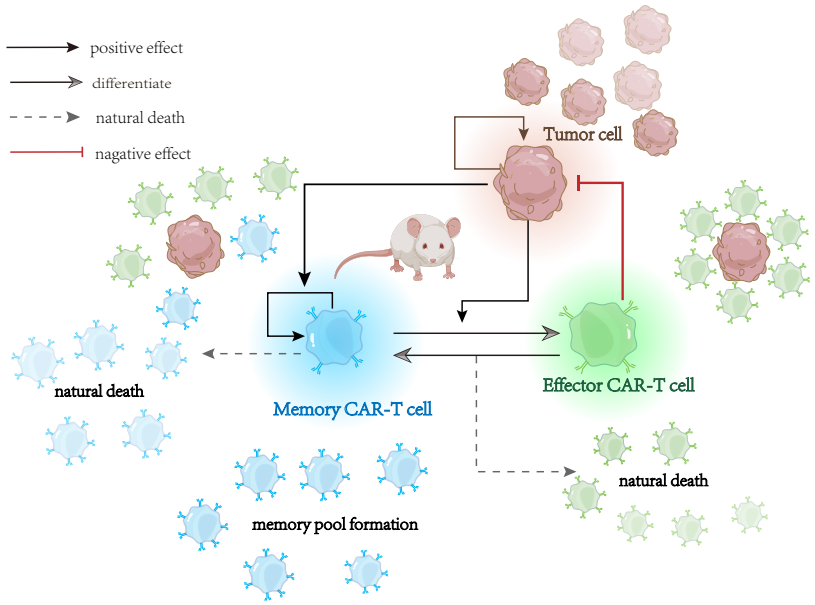

Figure 3. Schematic of the coarse-grained model. Effector CAR-T cells recognize and bind to tumor cells, forming complexes that signal effector CAR-T cells to release cytotoxic substances and kill tumor cells. Effector CAR-T cells can differentiate into memory CAR-T cells, which can self-proliferate and revert to effector CAR-T cells upon tumor cell stimulation.

Starting with an initial value of 1×10^6 tumor cells, based on animal experiments [11], we first set $T_E = T_M = 0$ to simulate tumor growth in the absence of CAR-T cells. The simulation indicated that, in the absence of CAR-T therapy, tumor cells grow rapidly, reaching a stable equilibrium of approximately 1.2×10^{10} cells within 30 days (Figure 4(a)).

Next, we introduced initial conditions of $T_E = 1 \times 10^7$ and $T_M = 1 \times 10^3$ to evaluate tumor growth under CAR-T therapy. The results demonstrated that CAR-T cells significantly reduced the tumor burden (Figure 4(b)). However, tumor cells rebounded rapidly by day 50, highlighting the recurrence process. After the initial reduction in tumor cells, the effector CAR-T cell count declined, while the number of memory CAR-T cells increased, illustrating differentiation from effector to memory cells (Figure 4(b)). At later stages of tumor cell recurrence, the number of memory CAR-T cells decreased and remained at a low level.

To better understand the impact of CAR-T cell infusion, we conducted simulations in which the initial values of T_E and T_M were varied to examine their influence on tumor growth dynamics. Specifically, T_M was fixed at 1×10^3, while T_E was varied from 2×10^6 to 2×10^7. The results revealed substantial differences in tumor progression associated with varying levels of T_E (Figure 4(c)). When the number of effector CAR-T cells was low, the tumor showed minimal response, indicating insufficient immune activity. In contrast, higher levels of effector CAR-T cells led to rapid recognition and binding to tumor cells, secretion of cytotoxic factors, and effective tumor cell elimination, thereby suppressing tumor growth.

Notably, when the initial number of effector CAR-T cells exceeded 0.9×10^7, a marked reduction in tumor burden was observed, indicating a successful tumor remission following CAR-T cell infusion. This finding suggests the existence of a critical threshold in the effector CAR-T cell population: only when this threshold is reached or surpassed can a robust anti-tumor response be initiated. Below this threshold, the CAR-T cell dose is insufficient to trigger an effective immune response, resulting in treatment failure and continued tumor progression.

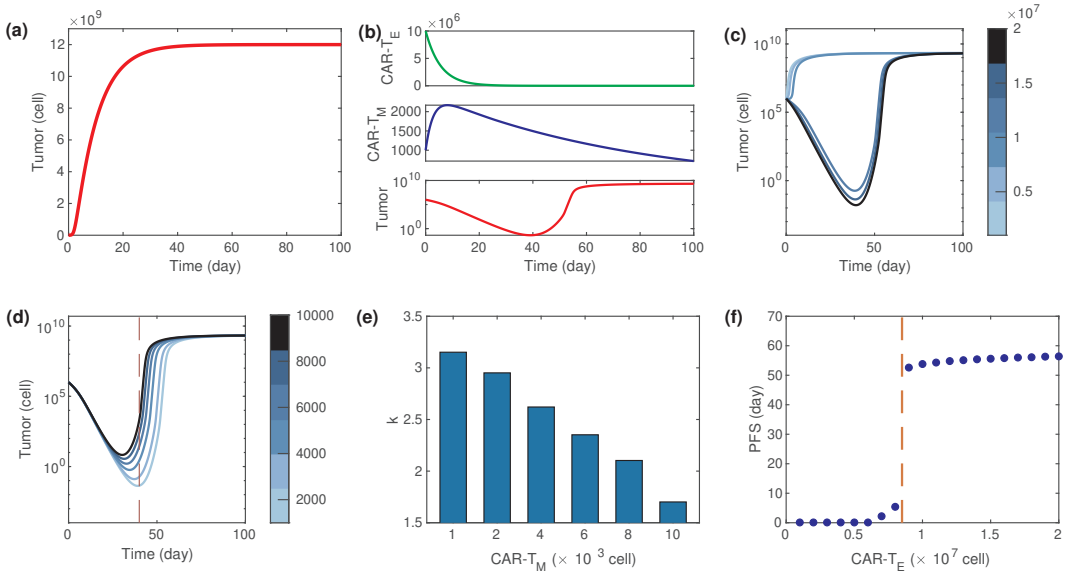

Figure 4. Evolution dynamics based on the coarse-grained model (3.1)–(3.3). (a) Tumor evolution dynamics in the absence of immunotherapy, with an initial tumor burden of 1×10^6. (b) Dynamics of effector and memory CAR-T cells and tumor cells under CAR-T therapy. The infused doses were 1×10^7 effector CAR-T cells and 1×10^3 memory CAR-T cells. (c) Tumor dynamics under varying effector CAR-T cell doses, ranging from 2×10^6 to 2×10^7, with memory CAR-T cells fixed at 1×10^3. (d) Tumor dynamics under varying memory CAR-T cell doses, ranging from 1×10^3 to 1×10^4, with effector CAR-T cells fixed at 1×10^7. (e) Tumor cell killing rate at day 40 as a function of infused memory CAR-T cell numbers, with effector CAR-T cells fixed at 1×10^7. (f) PFS as a function of infused effector CAR-T cell numbers, with memory CAR-T cells fixed at 1×10^3 and effector CAR-T cells varying from 1×10^6 to 2×10^7. The dashed line shows a threshold around 0.85×10^6. Parameter values: $\lambda_{T_{M\to E}} = 0.1 \times 10^{-5}$, $\lambda_{T_{E\to M}} = 0.26 \times 10^{-4}$, $\lambda_{T_M} = 0.02$, $\lambda_C = 3.3$, $K_C = 5 \times 10^7$, $k_{T_E} = 3.8$, $K_1 = 0.05$, $K_2 = 0.04$, $K_{T_{M_0}} = 0.2$, $K_{T_{M_1}} = 20$, $d_{T_E} = 0.18$, $d_{T_M} = 0.0065$, $d_C = 0.075$.

We next investigated how varying the initial number of memory CAR-T cells influences tumor control. The initial value of memory CAR-T cells was varied from 1×10^3 to 1×10^4, while the effector CAR-T cell count was fixed at 1×10^7. Surprisingly, increasing the number of memory CAR-T cells did not enhance tumor suppression; instead, it led to a noticeable reduction in PFS (Figure 4(d)). To elucidate the underlying mechanism, we examined the tumor cell killing rate, defined as

$$k(t) = k_{T_E}\frac{K_1T_E^*(t)}{1+K_1T_E^*(t)+K_2T_M^*(t)+K_1C(t)},$$

which depends on the relative abundances of effector and memory CAR-T cells, as well as the tumor cells. Notably, we observed marked differences in tumor dynamics on day 40, before the rapid phase of recurrence, for different levels of infused memory CAR-T cells (Figure 4(d)). Thus, we evaluated the tumor cell killing rate specifically at day 40.

As shown in Figure 4(e), the killing rate at day 40 decreased as the number of infused memory CAR-T cells increased. This reduction can be attributed to the competition between memory and effector CAR-T cells for binding to tumor cells. While memory CAR-T cells contribute to long-term immunity, they do not exert immediate cytotoxic effects. Therefore, an excessive number of memory CAR-T cells may limit effector cell access to tumor targets, thereby diminishing overall killing efficiency.

To further investigate how the number of infused CAR-T cells influences tumor progression, we fixed the memory CAR-T cell count at $T_M = 1\times10^3$ and varied the effector CAR-T cell dose from 1×10^6 to 2×10^7. The resulting PFS values revealed a sharp increase when the effector cell number exceeded approximately 0.9×10^6 (Figure 4(f)), indicating a threshold effect. Only when the number of infused effector CAR-T cells surpasses this critical level did the treatment result in meaningful tumor suppression. These findings, derived from the coarse-grained model, highlight the importance of optimizing CAR-T cell dosage to achieve maximal therapeutic efficacy.

3.3. Dynamics of CAR-T cell subtype numbers

We then analyzed the complete immune-tumor interaction model, governed by Eqs (2.1)–(2.13), with a particular focus on the dynamics of CAR-T cell subtypes following infusion. The initial conditions were set as follows: $CD4^+$ CAR-T cells at 1×10^4, pre-$CD8^+$ CAR-T cells at 1×10^7, effector CAR-T cells at 1×10^7, memory CAR-T cells at 1×10^3, and regulatory CAR-T cells at 1×10^3. The initial tumor cell count was 1×10^6 and the macrophage count was 1×10^2. Following CAR-T cell infusion, tumor cells declined rapidly, reaching remission by day 50. However, tumor recurrence was observed shortly thereafter (Figure 5(a)).

Each CAR-T cell subtype exhibited distinct dynamic behavior. $CD4^+$ CAR-T cells steadily declined, becoming nearly depleted by day 30 (Figure 5(b)). Pre-$CD8^+$ CAR-T cells expanded initially but underwent a sharp decline by day 15 (Figure 5(c)). Effector CAR-T cells followed a similar trend: rising in the early phase, then declining to low levels around day 50 (Figure 5(d)). Memory CAR-T cells increased gradually during the first 30 days and began to decline (Figure 5(e)). Regulatory CAR-T cells, which modulate immune responses, exhibited a continuous decline throughout the simulation (Figure 5(f)).

We also examined the dynamics of key cytokines. Because cytokines are secreted and degraded on a much faster timescale than cellular populations, we applied the quasi-equilibrium assumption to

express their concentrations in terms of cell populations, using Eqs (2.10)–(2.13). From these equations, it is evident that the dynamics of TGF-β, IL-2, and IL-6 closely follow those of tumor cells, CD4$^+$ CAR-T cells, and macrophages, respectively (Figure 5(g)). IFN-γ, which is primarily produced by effector and CD4$^+$ CAR-T cells and suppressed by regulatory CAR-T cells and TGF-β, shows an initial increase corresponding to effector cell expansion, followed by a gradual decline as effector cells diminish.

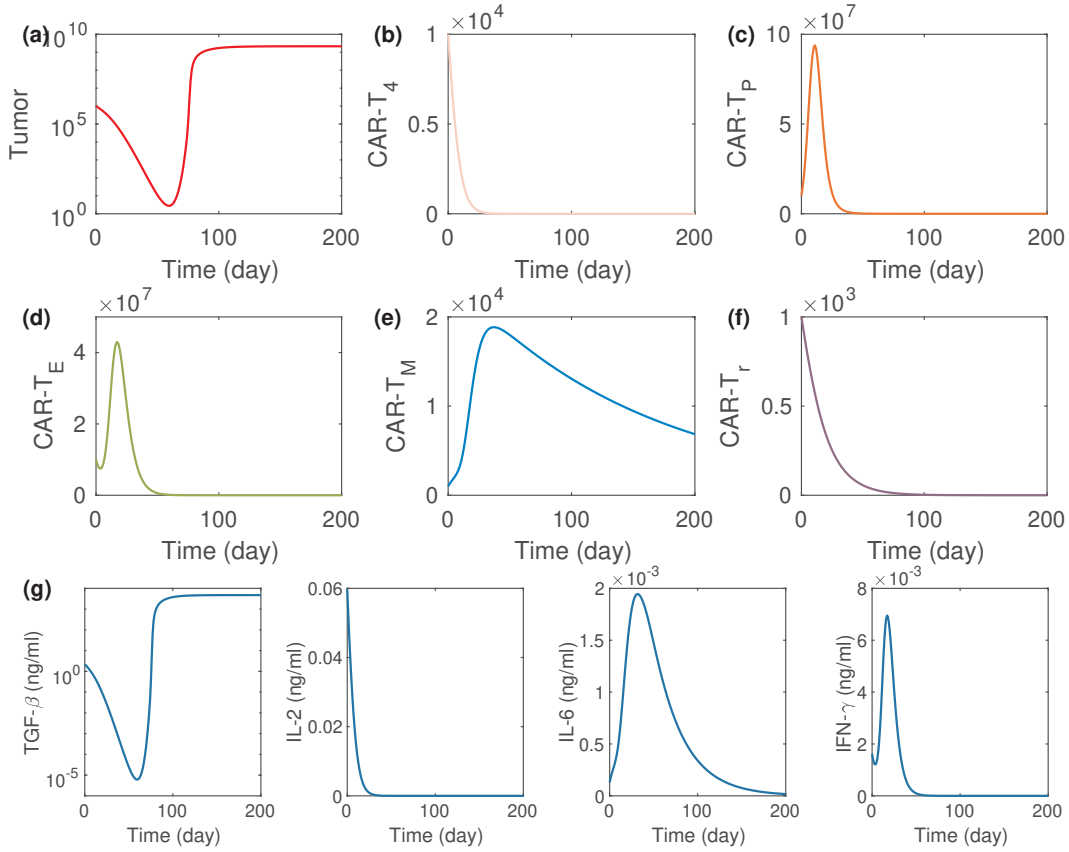

Figure 5. Dynamics of CAR- T cell subtypes and cytokines. (a) Tumor cell dynamics. (b) CD4$^+$ CAR-T cell dynamics. (c) Pre-CD8$^+$CAR-T cell dynamics. (d) Effector CAR-T cell dynamics. (e) Memory CAR-T cell dynamics. (f) Regulatory CAR-T cell dynamics. (g) Dynamics of the cytokines: TGF-β, IL-2, IL-6, and IFN-γ.

These results highlight the distinct functional roles of CAR-T cell subtypes in tumor control. CD4$^+$ CAR-T cells primarily act as early-phase immune activators, secreting cytokines to enhance the response before becoming depleted. Pre-CD8$^+$ CAR-T cells rapidly proliferate in response to immune signaling, differentiating into effector CAR-T cells, which are directly responsible for tumor elimination. As tumor burden decreases, a subset of effector CAR-T cells transition into memory CAR-T cells, ensuring long-term immune surveillance. Regulatory CAR-T cells contribute to immune homeostasis by preventing excessive immune activation, but gradually decline as the tumor regresses.

The recurrence of tumor growth following effector CAR-T cell exhaustion underscores the critical role of memory CAR-T cells in sustaining long-term immunity. Upon tumor reappearance, memory CAR-T cells can differentiate back into effector CAR-T cells, renewing their tumor-targeting activity

and contributing to prolonged disease control. These findings emphasize the importance of maintaining an optimal balance between effector and memory CAR-T cells to achieve durable therapeutic responses.

3.4. Tumor cell dynamics under different treatment options

The efficacy of CAR-T cell therapy is strongly influenced by the selection, dosage, and proportion of CAR-T cell subtypes. Optimizing these initial conditions is essential for improving therapeutic outcomes and developing more effective treatment strategies. Clinically, engineered T cells (CAR-T cells) are expanded in the laboratory before being infused back into the patient. Therefore, it is possible to control the number and composition of different cell subtypes during expansion and selection processes.

To assess how different CAR-T cell doses affect treatment outcomes, we used the initial conditions from Figure 5 as the control and increased each CAR-T subtype by 5-fold (treatment plan A, Figure 6(g)). Tumor progressions under these conditions are shown in Figure 6(a), with corresponding PFS in Figure 6(d). The results revealed that increasing $CD4^+$ CAR-T cells (A2) led to a significant increase in the PFS, while increases in pre-$CD8^+$ (A3), effector (A4), and memory CAR-T cells (A5) only marginally changed the PFS. Additionally, increasing regulatory CAR-T cells (A6) failed to induce tumor remission due to their immunosuppressive effects. These results highlight the need for careful regulation of CAR-T cell levels for improved tumor suppression.

Next, we examined the impact of varying the total CAR-T cell dose while maintaining fixed subtype proportions (treatment plan B, Figure 6(g)). Tumor progression with total doses ranging from 1×10^6 to 25×10^6 is shown in Figure 6(b). A threshold effect was observed: therapy was effective only when the total CAR-T cell count exceeded 5×10^6 (Figure 6(e)). Moreover, increasing the dose beyond 10×10^6 did not further extend PFS and instead led to diminished therapeutic benefits, underscoring the importance of optimizing both dose and proportions to maximize efficacy.

We further investigated how altering CAR-T subtype proportions affect treatment outcomes while keeping the total infused dose constant (treatment plan C, Figure 6(g)). Six scenarios were considered: increasing $CD4^+$ while reducing memory CAR-T cells (C1), increasing memory while decreasing $CD4^+$ CAR-T cells (C4), increasing pre-$CD8^+$ while reducing effector CAR-T cells (C2), and vice versa (C5). Additionally, we tested increasing both $CD4^+$ and pre-$CD8^+$ CAR-T cells with compensatory reductions in memory and effector CAR-T cells (C3 and C6). The tumor cell dynamics under these conditions are shown in Figure 6(c). The results indicated that increasing effector CAR-T cells (C5 & C6) provides superior therapeutic effects, as reflected in extended PFS (Figure 6(f)).

These findings provide key insights into CAR-T cell therapy optimization. High doses of $CD4^+$ CAR-T cells enhance cytokine secretion, promoting the proliferation, activation, and survival of effector and pre-$CD8^+$ CAR-T cells. Increasing pre-$CD8^+$ CAR-T cells supports sustained anti-tumor activity by generating new effector cells *in vivo*. In contrast, excessive memory CAR-T cells may saturate tumor antigen-binding sites, impeding effector cell function, while an overabundance of effector cells can lead to immune overactivation and depletion. Thus, carefully increasing $CD4^+$ and pre-$CD8^+$ CAR-T cells while maintaining a balanced proportion of other subtypes can significantly enhance therapeutic efficacy.

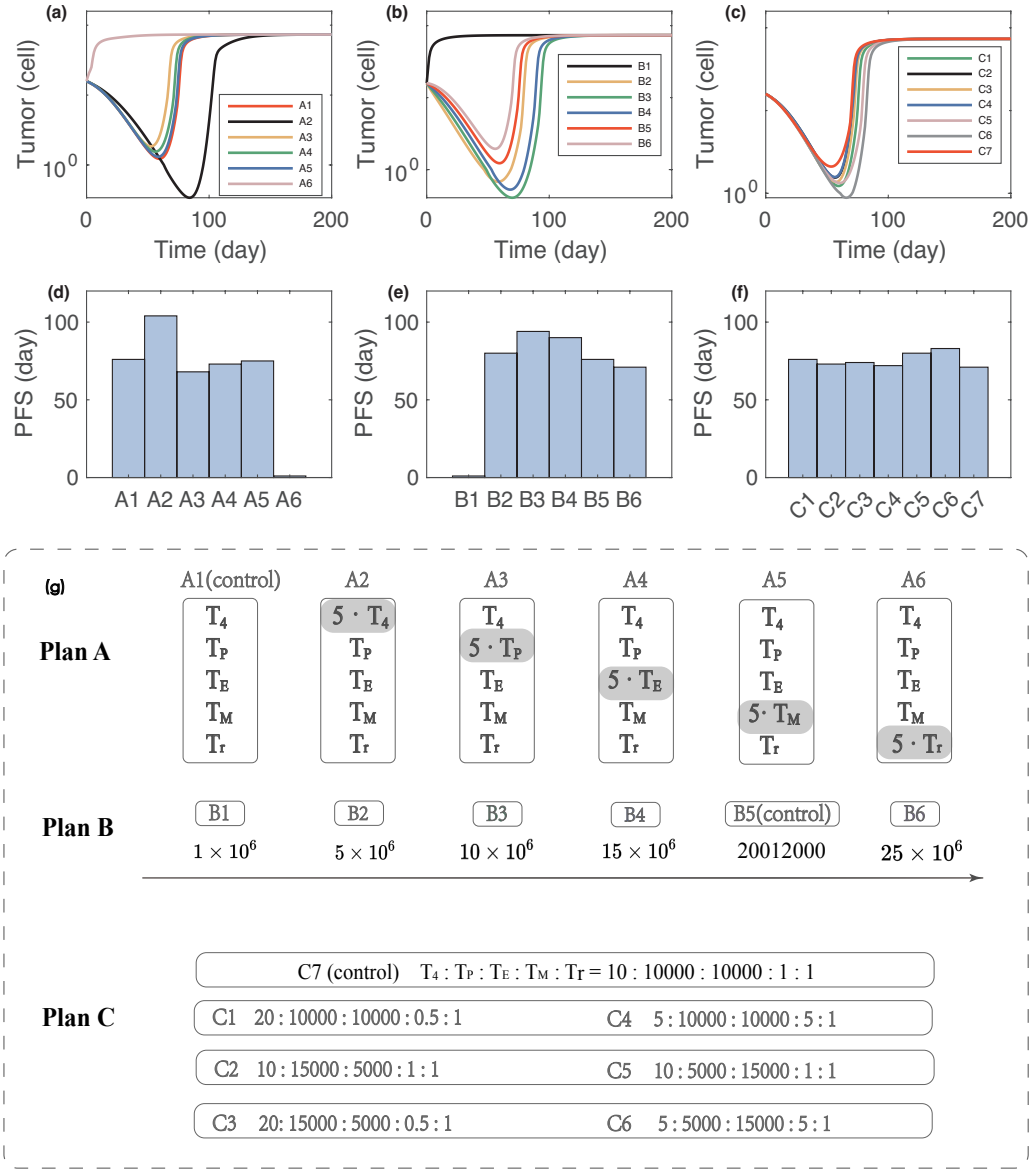

Figure 6. Tumor progression under different treatment scenarios. (a) Tumor cell dynamics under protocols with a 5-fold increase in each CAR-T cell subtype. (b) Tumor cell dynamics with varying total CAR-T cell numbers while maintaining constant subtype proportions. (c) Tumor cell dynamics with CAR-T subtype proportions, keeping the total number unchanged. (d) Progression-free survival (PFS) for a 5-fold increase in each CAR-T cell subtype. (e) PFS with varying total CAR-T cell numbers. (f) PFS with different CAR-T cell subtype proportions. (g) Treatment plans, where A1, B5, and C7 represent the control plan from Figure 5. Control plans are shown in red in (a), (b), and (c).

3.5. Optimization strategies for CAR-T cell dosing based on tumor burden

To optimize CAR-T cell dosing in response to varying tumor burdens, we applied the Particle Swarm Optimization (PSO) algorithm to determine the optimal total doses and subtype distributions

of CAR-T cells for initial tumor cell counts ranging from 1×10^6 to 6×10^6. For each given initial tumor cell count, the optimal doses of CAR-T cell subtypes were determined using the PSO algorithm to maximize PFS. PSO is an iterative, population-based computational technique that explores the solution space by adjusting the positions and velocities of candidate solutions (particles) based on their individual and collective experiences. This method enables adaptive optimization of CAR-T dosing regimens to different tumor burdens.

As shown in Figure 7(a)–(f), the total CAR-T cell dose increases proportionally with tumor burden (Figure 7(a)). Specifically, the numbers of $CD4^+$, pre-$CD8^+$, effector, and memory CAR-T cells scaled with tumor burden (Figure 7(b)–(e)), whereas the number of regulatory CAR-T cells remains nonlinearly dependent on the tumor cell count when the number is small and relatively constant when the tumor cell count is larger than 2.3×10^6 (Figure 7(f)). Notably, the PFS under PSO-optimized dosing varied consistently between 70 and 100 days across all tumor sizes (Figure 7(g)), outperforming most dosing strategies shown in Figure 6. These findings demonstrate the effectiveness of PSO-derived dosing strategies in adapting to tumor burden, thereby maintaining robust therapeutic outcomes.

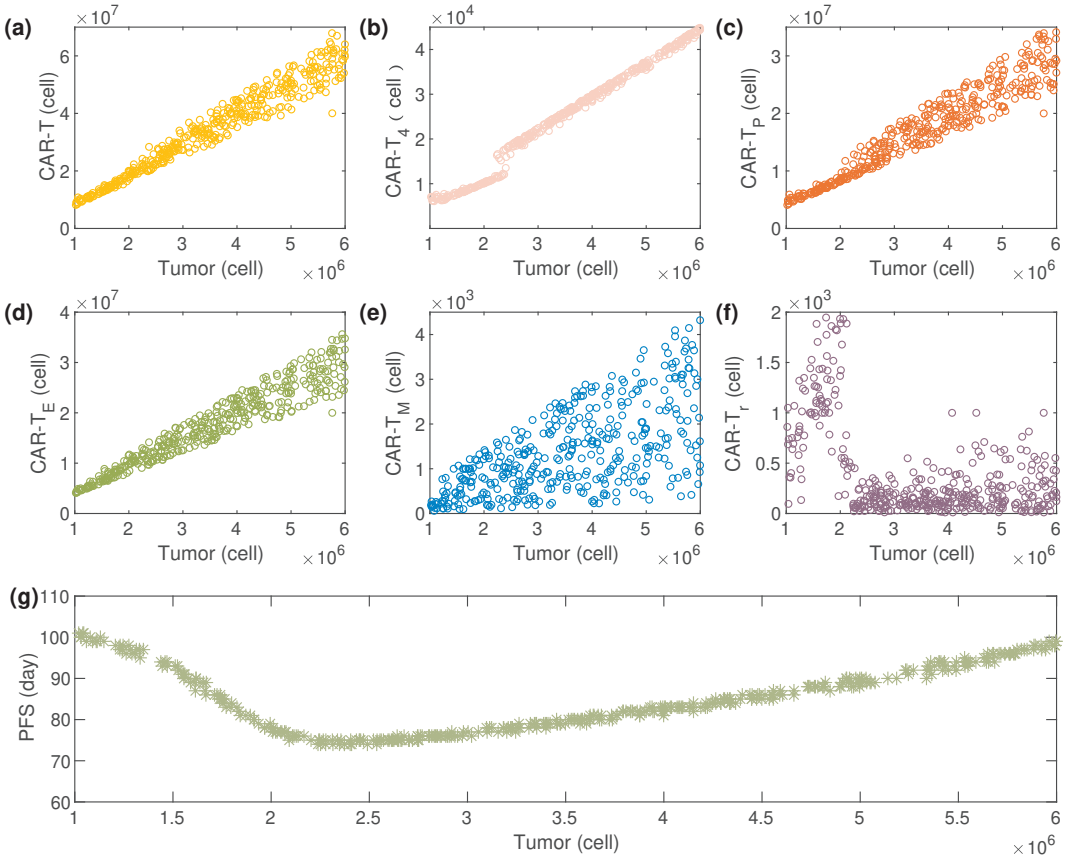

Figure 7. Optimal CAR-T cell doses for varying tumor burdens. (a)–(f) PSO-optimized total and subtype-specific CAR-T cell doses for different initial tumor sizes. (g) PFS under PSO-optimized dosing across varying tumor burdens.

The dynamics of CAR-T cell subtypes and cytokines following administration of the PSO-optimized doses are illustrated in Figure 8. Under this optimized regimen, PFS was extended from 76 (as shown in Figure 5) to 101 days. Compared to the previous dosing strategy, the optimized regi-

men results in overall lower levels of CAR-T cells. Consequently, the levels of cytokines IL-2, IL-6, and IFN-γ are also reduced under the optimized strategy.

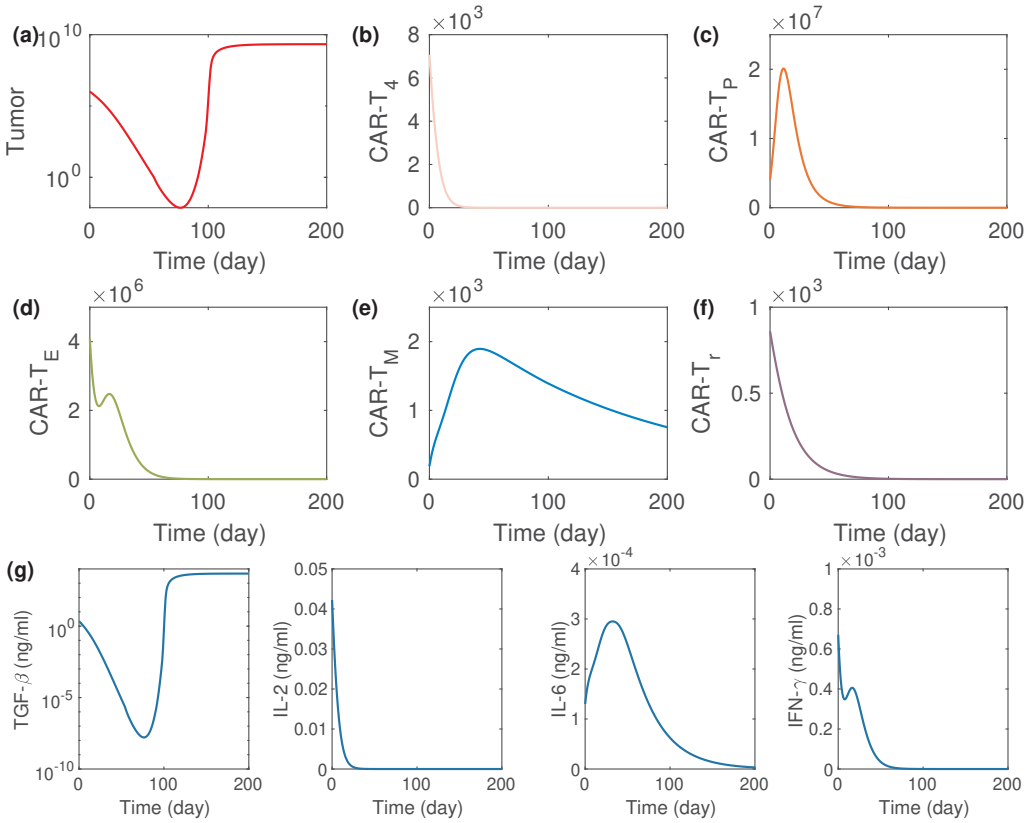

Figure 8. Dynamics of CAR-T cell subtypes and cytokines under the optimized dosing strategy. (a) Tumor cell population. (b) CD4$^+$ CAR-T cells. (c) Pre-CD8$^+$ CAR-T cells. (d) Effector CAR-T cells. (e) Memory CAR-T cells. (f) Regulatory CAR-T cells. (g) Cytokine levels: TGF-β, IL-2, IL-6, and IFN-γ. Initial values of CAR-T subtypes correspond to PSO-optimized doses, with an initial tumor burden of 1×10^6.

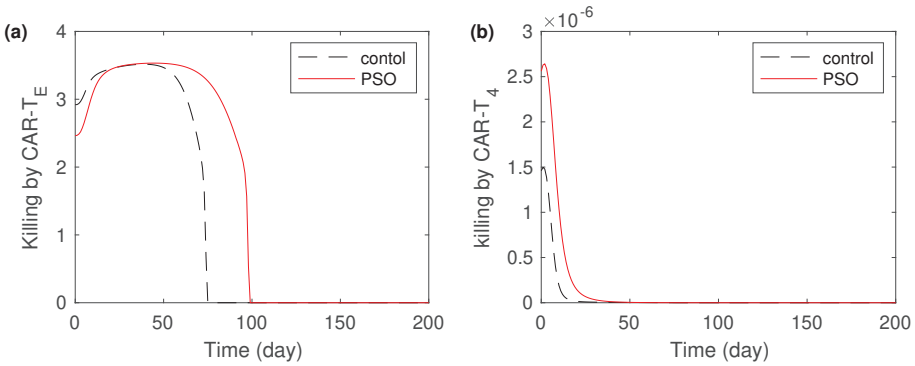

Figure 9. Evolution of CAR-T cell killing rates. (a) Killing rate of effector CAR-T cells. (b) Killing rate of CD4$^+$ CAR-T cells. Control refers to results based on the default initial CAR-T cell doses as in Figure 5, while PSO corresponds to results based on the PSO-optimized doses as in Figure 8.

To understand the mechanism underlying the extended PFS achieved by the optimized doses, we calculated the tumor cell killing rates mediated by effector and CD4$^+$ CAR-T cells. These killing rates are given by

$$k_{T_E}\frac{K_1T_E}{1+K_1T_E^*+K_2T_M^*+K_3T_4^*+K_1C}\times\frac{1}{1+T_r/K_{T_r}} \tag{3.4}$$

and

$$k_{T_4}\frac{K_3T_4}{1+K_1T_E^*+K_2T_M^*+K_3T_4^*+K_1C}\times\frac{1}{1+T_r/K_{T_r}}, \tag{3.5}$$

respectively. A comparison of these killing rates is shown in Figure 9. The killing rate mediated by effector CAR-T cells is markedly higher than that of CD4$^+$ CAR-T cells and exhibits a more sustained effect under the PSO-optimized doses. From Eqs (3.4) and (3.5), it is evident that the presence of memory and regulatory CAR-T cells tends to suppress tumor cell killing. Notably, the optimized regimen results in lower levels of both memory and regulatory CAR-T cells (Figure 8). These results suggest that effector CAR-T cells are primarily responsible for tumor cell elimination and that the optimized dosing strategy prolongs their killing efficacy by minimizing the inhibitory influence of memory and regulatory CAR-T cells.

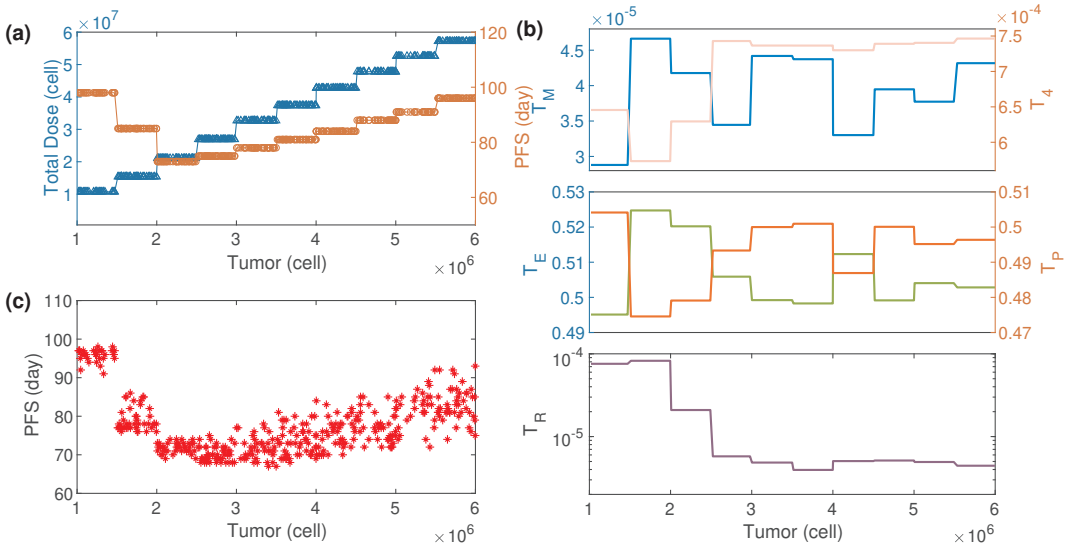

Figure 10. Optimal CAR-T cell dosing strategies. (a) Averaged CAR-T cell doses and the corresponding PFS based on the PSO-optimized protocol for different tumor burdens. (b) Propotions of CAR-T cell subtypes relative to the total dose across varying tumor burdens. (c) PFS outcomes corresponding to different CAR-T cell subtype proportions.

Furthermore, to address the challenges of precise dosing control in clinical settings, we developed a simplified dosing plan by averaging the PSO-optimized CAR-T doses over tumor cell intervals of 0.5×10^6. This approach maintained a consistent PFS of approximately 70–100 days (Figure 10(a)), indicating that even a streamlined dosing strategy can effectively suppress tumors across varying tumor burdens.

Additionally, we explored an alternative dosing strategy based on the proportion of each CAR-T cell subtype relative to the total dose. The optimal proportion ranges for each subtype were as follows (Figure 10(b)): CD4$^+$ CAR-T cells: 5.6×10^{-4}–7.6×10^{-4}; pre-CD8$^+$ CAR-T cells: 0.47–0.51;

effector CAR-T cells: 0.49–0.53; memory CAR-T cells: 2.8×10^{-5}–4.8×10^{-5}; and regulatory CAR-T cells: 0.2×10^{-5}–1×10^{-4}. When CAR-T cells were administered using the total doses shown in Figure 10, with the subtype proportions randomly sampled within the ranges above, the resulting PFS remained between 65 and 100 days (Figure 8(c)), demonstrating the robustness of this proportional dosing strategy.

These findings suggest that adjusting CAR-T cell doses to match specific tumor burdens using PSO-optimized strategies or simplified dosing based on subtype proportions can significantly enhance treatment outcomes. Both approaches offer practical and effective strategies for optimizing CAR-T therapy across diverse tumor scenarios.

4. Discussion

CAR-T cell therapy has revolutionized cancer immunotherapy, underscoring the need for mathematical models that capture tumor-immune interactions. In this study, we developed a dynamic network model of the tumor-immune microenvironment, incorporating the bidirectional regulation between tumor cells and immune cells. Our model quantitatively describes key processes such as cell proliferation, differentiation, apoptosis, and immune-mediated tumor elimination, while also integrating cytokine and cellular dynamics. Initially, we constructed a model with three CAR-T cell subtypes to simulate treatment responses and drug-resistant relapse in cancer patients. We then extended it to five CAR-T cell subtypes and employed the PSO algorithm to determine optimal CAR-T dosages and subtype distributions for effective CAR-T therapy.

Mathematical modeling provides critical insights into tumor dynamics by quantitatively describing interactions among tumor cells, immune cells, and cytokines. However, modeling CAR-T cell immunotherapy remains challenging due to its complexity. Existing models often focus on effector and memory CAR-T cells, overlooking other clinically relevant subtypes. Our work advances the field by developing a mathematical model that captures the intricate regulatory network governing tumor dynamics and immune responses. By leveraging PSO-based optimization, we identified personalized dosing strategies that enhance therapeutic efficacy. These findings provide valuable insights for optimizing CAR-T therapies and developing more effective treatment protocols.

CAR-T cell therapy has revolutionized cancer treatment, particularly for hematologic malignancies. However, its clinical success is often constrained by the complexity of CAR-T kinetics, drug metabolism, and intricate tumor-immune interactions. Tumor immune evasion strategies, coupled with the immunosuppressive microenvironment response, further compromise CAR-T cell efficacy, leading to exhaustion and diminished therapeutic response. Additionally, severe adverse effects such as cytokine release syndrome (CRS) and neurotoxicity pose significant challenges to treatment safety [47]. Overcoming these limitations is crucial for enhancing both the efficacy and safety of CAR-T cell therapies, paving the way for more durable and effective treatment strategies.

Ongoing advances in cancer biology, immunology, and bioengineering are driving the evolution of CAR-T cell therapies. Genetic engineering strategies, including receptor modifications and combination therapies, can enhance CAR-T cell persistence and tumor-killing capacity. Efforts to mitigate CAR-T-associated toxicities include the design of safer CAR constructs, the incorporation of safety switches, and cytokine modulation to reduce inflammatory side effects [48]. Future research should integrate these therapeutic innovations into mathematical models to better capture the complexity of

CAR-T therapy. Incorporating clinical data and high-throughput bioinformatics data will further refine these models, improving their predictive power and translational relevance. Validating the models across diverse patient populations will be essential for ensuring their clinical applicability.

In this study, we employed a combination of coarse-grained and detailed mathematical models to optimize CAR-T cell dosing strategies in response to varying tumor burdens. By using the PSO algorithm, we identified optimal CAR-T cell doses and subtype distributions that maximize PFS across different tumor sizes. Our findings suggest that tailored dosing strategies, which consider the dynamic interplay between CAR-T cell subtypes, can significantly improve therapeutic outcomes. Specifically, increasing $CD4^+$ and pre-$CD8^+$ CAR-T cells while adjusting memory and effector cell proportions enhances treatment efficacy, leading to prolonged PFS.

However, our study has several limitations. The proposed model does not account for severe side effects such as CRS and neurotoxicity, which are critical considerations in CAR-T cell therapy. Incorporating these adverse effects into the model would introduce additional constraints when determining the optimal therapeutic strategy. Furthermore, the model does not fully capture the complex dynamics of the tumor microenvironment, particularly the role of endogenous immune cells. The interactions between endogenous immune cells and infused CAR-T cells significantly influence treatment efficacy and should be considered in future refinements. Additionally, our findings are based on computational simulations and require validation with experimental or clinical data. Future research should focus on integrating empirical data to enhance model accuracy and improve its predictive capabilities.

Use of AI tools declaration

The authors declare they have not used Artificial Intelligence (AI) tools in the creation of this article.

Acknowledgments

This work was supported by the National Natural Science Foundation of China (NSFC 12331018).

Data availability

The program code and simulation results are available from https://github.com/jinzhilei/CAR-T-Optimal.

Conflict of interest

Jinzhi Lei is an editorial board member for Mathematical Biosciences and Engineering and was not involved in the editorial review or the decision to publish this article. All authors declare that there are no competing interests.

References

1. P. Abrisqueta, New insights into first-line therapy in diffuse large B-cell lymphoma: Are we improving outcomes, *J. Clin. Med.*, **13** (2024), 1929. https://doi.org/10.3390/jcm13071929

2. J. A. Fraietta, C. L. Nobles, M. A. Sammons, S. Lundh, S. A. Carty, T. J. Reich, et al., Disruption of TET2 promotes the therapeutic efficacy of CD19-targeted T cells, *Nature*, **558** (2018), 307–312. https://doi.org/10.1038/s41586-018-0178-z

3. R. A. Gardner, O. Finney, C. Annesley, H. Brakke, C. Summers, K. Leger, et al., Intent-to-treat leukemia remission by CD19 CAR T cells of defined formulation and dose in children and young adults, *Blood*, **129** (2017), 3322–3331. https://doi.org/10.1182/blood-2017-02-769208

4. C. H. June, R. S. O'Coonor, O. U. Kawalekar, S. Ghassemi, M. C. Milone, CAR T cell immunotherapy for human cancer, *Science*, **359** (2018), 1361–1365. https://doi.org/10.1126/science.aar6711

5. G. Gross, T. Waks, Z. Eshhar, Expression of immunoglobulin-T-cell receptor chimeric molecules as functional receptors with antibody-type specificity, *Proc. Natl. Acad. Sci. U.S.A.*, **86** (1989), 10024–10028. https://doi.org/10.1073/pnas.86.24.10024

6. S. S. Neelapu, F. L. Locke, N. L. Bartlett, L. J. Lekakis, D. B. Miklos, et al., Axicabtagene ciloleucel CAR T-cell therapy in refractory large B-cell lymphoma, *N. Engl. J. Med.*, **377** (2017), 2531–2544. https://doi.org/10.1056/NEJMoa1707447

7. S. J. Schuster, M. R. Bishop, C. S. Tam, E. K. Waller, P. Borchmann, J. P. McGuirk, et al., Tisagenlecleucel in adult relapsed or refractory diffuse large B-cell lymphoma, *N. Engl. J. Med.*, **380** (2017), 45–56. https://doi.org/10.1056/NEJMoa1804980

8. P. Dreger, P. Corradini, J. G. Gribben, B. Glass, M. Jerkeman, M. J. Kersten, et al., CD19-directed CAR T cells as first salvage therapy for large B-cell lymphoma: towards a rational approach, *Lancet Haematol.*, **10** (2023), e1006–e1015. https://doi.org/10.1016/S2352-3026(23)00307-1

9. G. Gross, Z. Eshhar, Therapeutic potential of T cell chimeric antigen receptors (CARs) in cancer treatment: counteracting off-tumor toxicities for safe CAR T cell therapy, *Annu. Rev. Pharmacol. Toxicol.*, **56** (2016), 59–83. https://doi.org/10.1146/annurev-pharmtox-010814-124844

10. M. Hudecek, M. Lupo-Stanghellini, P. L. Kosasih, D. Sommermeyer, M. C. Jensen, C. Rader, et al., Receptor affinity and extracellular domain modifications affect tumor recognition by ROR1-specific chimeric antigen receptor T cells, *Clin. Cancer Res.*, **19** (2013), 3153–3164. https://doi.org/10.1158/1078-0432.CCR-13-0330

11. C. Zhang, C. Shao, X. Jiao, Y. Bai, M. Li, H. Shi, et al., Individual cell-based modeling of tumor cell plasticity-induced immune escape after CAR-T therapy, *Comput. Syst. Oncol.*, **1** (2021), e21029. https://doi.org/10.1002/cso2.1029

12. E. R. Swanson, E. Köse, E. A. Zollinger, S. L. Elliott, Mathematical modeling of tumor and cancer stem cells treated with CAR-T therapy and inhibition of TGF-β, *Bull. Math. Biol.*, **84** (2022), 58. https://doi.org/10.1007/s11538-022-01015-5

13. Y. Bulliard, B. S. Andersson, M. A. Baysal, J. Damiano, A. M. Tsimberidou, Reprogramming T cell differentiation and exhaustion in CAR-T cell therapy, *J. Hematol. Oncol.*, **16** (2023), 108. https://doi.org/10.1186/s13045-023-01504-7

14. P. Sahoo, X. Yang, D. Abler, D. Maestrini, V. Adhikarla, D. Frankhouser, et al., Mathematical deconvolution of CAR T-cell proliferation and exhaustion from real-time killing assay data, *J. R. Soc. Interface*, **17** (2020), 20190734. https://doi.org/10.1098/rsif.2019.0734

15. D. C. Kirouac, C. Zmurchok, D. Morris, Making drugs from T cells: The quantitative pharmacology of engineered T cell therapeutics, *NPJ Syst. Biol. Appl.*, **10** (2024), 31. https://doi.org/10.1038/s41540-024-00355-3

16. L. R. C. Barros, E. A. Paixão, A. M. P. Valli, G. T. Naozuka, A. C. Fassoni, R. C. Almeida, CARTmath-A mathematical model of CAR-T immunotherapy in preclinical studies of hematological cancers, *Cancers (Basel)*, **13** (2021), 2941. https://doi.org/10.3390/cancers13122941

17. E. A. Paixão, L. R. C. Barros, A. C. Fassoni, R. C. Almeida, Modeling patient-specific CAR-T Cell dynamics: multiphasic kinetics via phenotypic differentiation, *Cancers (Basel)*, **14** (2022), 5576. https://doi.org/10.3390/cancers14225576

18. C. J. Turtle, L. Hanafi, C. Berger, T. A. Gooley, S. Cherian, M. Hudecek, et al., CD19 CAR–T cells of defined CD4+:CD8+ composition in adult B cell ALL patients, *J. Clin. Invest.*, **126** (2016), 2123–2138. https://doi.org/10.1172/JCI85309

19. M. Ruella, M. Klichinsky, S. S. Kenderian, O. Shestova, A. Ziober, D. O. Kraft, et al., Overcoming the immunosuppressive tumor microenvironment of Hodgkin lymphoma using chimeric antigen receptor T cells, *Cancer Discov.*, **7** (2017), 1154–1167. https://doi.org/10.1158/2159-8290.CD-16-0850

20. F. Crauste, J. Mafille, L. Boucinha, S. Djebali, O. Gandrillon, J. Marvel, et al., Identification of nascent memory CD8 T cells and modeling of their ontogeny, *Cell Syst.*, **4** (2017), 306–317. https://doi.org/10.1016/j.cels.2017.01.014

21. J. N. Brudno, J. N. Kochenderfer, Chimeric antigen receptor T-cell therapies for lymphoma, *Nat. Rev. Clin. Oncol.*, **15** (2018), 31–46. https://doi.org/10.1038/nrclinonc.2017.128

22. D. Sommermeyer, T. Hill, S. M. Shamah, A. I. Salter, Y. Chen, K. M. Mohler, et al., Fully human CD19-specific chimeric antigen receptors for T-cell therapy, *Leukemia*, **31** (2017), 2191–2199. https://doi.org/10.1038/leu.2017.57

23. L. Adam, N. N. Shah, Chimeric antigen receptor modified T cell therapy in B cell non-Hodgkin lymphomas, *Am. J. Hematol.*, **94** (2019), S18–S23. https://doi.org/10.1002/ajh.25403

24. X. Zhang, L. Zhu, H. Zhang, S. Chen, Y. Xiao, CAR-T cell therapy in hematological malignancies: current opportunities and challenges, *Front. Immunol.*, **13** (2022), 927153. https://doi.org/10.3389/fimmu.2022.927153

25. J. Zhu, W. E. Paul, CD4 T cells: fates, functions, and faults, *Blood*, **112** (2008), 1557–1569. https://doi.org/10.1182/blood-2008-05-078154

26. S. M. Kaech, W. Cui, Transcriptional control of effector and memory CD8+ T cell differentiation, *Nat. Rev. Immunol.*, **12** (2012), 749–761. https://doi.org/10.1038/nri3307

27. S. Kang, T. Kishimoto, Interplay between interleukin-6 signaling and the vascular endothelium in cytokine storms, *Exp. Mol. Med.*, **53** (2021), 1116–1123. https://doi.org/10.1038/s12276-021-00649-0

28. A. T. Gacerez, C. L. Sentman, T-bet promotes potent antitumor activity of $CD4^+$ CAR T cells, *Cancer Gene Ther.*, **25** (2018), 117–128. https://doi.org/10.1038/s41417-018-0012-7

29. Z. Good, J. Y. Spiegel, B. Sahaf, M. B. Malipatlolla, Z. J. Ehlinger, S. Kurra, et al., Post-infusion CAR TReg cells identify patients resistant to CD19-CAR therapy, *Nat. Med.*, **28** (2022), 1860–1871. https://doi.org/10.1038/s41591-022-01960-7

30. S. Faude, J. Wei, K. Muralidharan, X. Xu, G. Mertheim, M. Paessler, et al., Absolute lymphocyte count proliferation kinetics after CAR T-cell infusion impact response and relapse, *Blood Adv.*, **5** (2021), 2128–2136. https://doi.org/10.1182/bloodadvances.2020004038

31. S. N. Mueller, L. K. Mackay, Tissue-resident memory T cells: local specialists in immune defence, *Nat. Rev. Immunol.*, **16** (2015), 79089. https://doi.org/10.1038/nri.2015.3

32. B. Youngblood, J. S. Hale, H. T. Kissick, E. Ahn, X. Xu, A. Wieland, et al., Effector CD8 T cells dedifferentiate into long-lived memory cells, *Nature*, **552** (2017), 404–409. https://doi.org/10.1038/nature25144

33. R. S. Akondy, M. Fitch, S. Edupuganti, S. Yang, H. T. Kissick, K. W. Li, et al., Origin and differentiation of human memory CD8 T cells after vaccination, *Nature*, **552** (2017), 362–367. https://doi.org/10.1038/nature24633

34. C. Raffin, L. T. Vo, J. A. Bluestone, T_{reg} cell-based therapies: challenges and perspectives, *Nat. Rev. Immunol.*, **20** (2020), 158–172. https://doi.org/10.1038/s41577-019-0232-6

35. S. Z. Josefowicz, L. F. Lu, A. Y. Rudensky, Regulatory T cells: mechanisms of differentiation and function, *Annu. Rev. Immunol.*, **30** (2012), 531–564. https://doi.org/10.1146/annurev.immunol.25.022106.141623

36. N. J. Haradhvala, M. B. Leick, K. Maurer, S. H. Gohil, R. C. Larson, N. Yao, et al., Distinct cellular dynamics associated with response to CAR-T therapy for refractory B cell lymphoma, *Nat. Med.*, **28** (2022), 1848–1859. https://doi.org/10.1038/s41591-022-01959-0

37. X. Li, J. Henderson, M. J. Gordon, I. Sheikh, L. J. Nastoupil, J. Westin, et al., A single-cell atlas of CD19 chimeric antigen receptor T cells, *Cancer*, **41** (2023), 1835–1837. https://doi.org/10.1016/j.ccell.2023.08.015

38. J. Lei, A general mathematical framework for understanding the behavior of heterogeneous stem cell regeneration, *J. Theor. Biol.*, **492** (2020), 110196. https://doi.org/10.1016/j.jtbi.2020.110196

39. S. Bernard, J. Bélair, M. C. Mackey, Oscillations in cyclical neutropenia: new evidence based on mathematical modeling, *J. Theor. Biol.*, **223** (2003), 283–298. https://doi.org/10.1016/S0022-5193(03)00090-0

40. J. Li, J. Wu, J. Zhang, L. Tang, H. Mei, Y. Hu, et al., A multicompartment mathematical model based on host immunity for dissecting COVID-19 heterogeneity, *Heliyon*, **8** (2022), e09488. https://doi.org/10.1016/j.heliyon.2022.e09488

41. X. Lai, A. Friedman, Combination therapy for melanoma with BRAF/MEK inhibitor and immune checkpoint inhibitor: a mathematical model, *BMC Syst. Biol.*, **11** (2017), 70. https://doi.org/10.1186/s12918-017-0446-9

42. M. Robertson-Tessi, A. El-Kareh, A. Goriely, A mathematical model of tumor-immune interactions, *J. Theor. Biol.*, **2012** (2012), 56–73. https://doi.org/10.1016/j.jtbi.2011.10.027

43. W. Lo, R. I. Arsenescu, A. Friedman, Mathematical model of the roles of T cells in inflammatory bowel disease, *Bull. Math. Biol.*, **75** (2013), 1417–1433. https://doi.org/10.1007/s11538-013-9853-2

44. K. E. Johnson, Y. Makanji, P. Temple-Smith, E. K. Kelly, P. A. Barton, S. L. Al-Musawi, et al., Biological activity and *in vivo* half-life of pro-activin A in male rats, *Mol. Cell Endocrinol.*, **422** (2016), 84–92. https://doi.org/10.1016/j.mce.2015.12.007

45. K. A. Foon, S. A. Sherwin, P. G. Abrams, H. C. Stevenson, P. Holmes, A. E. Maluish, et al., A phase I trial of recombinant gamma interferon in patients with cancer, *Cancer Immunol. Immunother.*, **20** (1985), 193–197. https://doi.org/10.1007/BF00205575

46. C. Li, Z. Ren, G. Yang, J. Lei, Mathematical modeling of tumor immune interactions: the role of anti-FGFR and anti-PD-1 in the combination therapy, *Bull. Math. Biol.*, **86** (2024), 116. https://doi.org/10.1007/s11538-024-01329-6

47. H. Wang, L. Tang, Y. Kong, W. Liu, X. Zhu, Y. You, Strategies for reducing toxicity and enhancing efficacy of chimeric antigen receptor T cell therapy in hematological malignancies, *Int. J. Mol. Sci.*, **24** (2023), 9115. https://doi.org/10.3390/ijms24119115

48. J. Huang, X. Huang, J. Huang, CAR-T cell therapy for hematological malignancies: Limitations and optimization strategies, *Front. Immunol.*, **13** (2022), 1019115. https://doi.org/10.3389/fimmu.2022.1019115

AIMS Press